published in Morskoy Gidrofizicheskiy Zhurnal, 2025, Vol. 41, Iss. 5, pp. 658-680

Original article

Modeling of River Plume Propagation in the Coastal Zone of Non-Tidal Sea

M. V. Tsyganova [™], E. M. Lemeshko, V. V. Fomin, Yu. N. Ryabtsev

Marine Hydrophysical Institute of RAS, Sevastopol, Russian Federation

□ m.tsvganova@mhi-ras.ru

Abstract

Purpose. The purpose of the work is to investigate the propagation of river waters as they flow into the sea, the formation of plume and coastal buoyancy currents as well as to assess the plume characteristics and their evolution parameters depending on river discharge and hydrological conditions of the Black Sea northwestern shelf in the absence of wind forcing.

Methods and Results. The plume formation and propagation were studied by numerical simulation based on the POM three-dimensional σ-coordinate numerical model applied to calculate circulation in the coastal zone with due regard for river runoff. The performed series of numerical experiments took into account the impact of both river seasonal changes in discharge and salinity and the seawater stratification on plume dynamics within the range of Froude numbers up to 1. The calculations were performed for a rectangular area. The average climatic data on river discharge, sea- and fresh-water temperature and salinity were used as the model input parameters. The quantitative estimates of plume characteristics and evolution parameters as well as its depth, radius and center position depending on the balance of buoyancy forces (Burger number) and inertia (Froude and Rossby numbers) were obtained. They are consistent with the data of hydrological observations carried out under conditions of weak winds, with their speed less than 5 m/s. Application of the TVD schemes in the model has provided monotonicity of numerical solutions for areas with high spatial gradients in hydrophysical parameters and also reduced computational viscosity significantly. It has been established that the discharges of freshwater transported by the coastal current are proportional to the square of its available potential energy; the dependence is described by a linear regression equation with high determination (~ 0.95) and correlation (~ 0.97) coefficients.

Conclusions. The obtained relationships for plume depth and width and coastal current discharge can be used for assessing these parameters based on hydrological information or satellite data at a wind speed of less than 5 m/s. On average, after ~ 10 days, a quasi-stationary regime is formed, in which the coastal current discharge stabilizes at $\sim 40\%$ of the river discharge, while the remaining $\sim 60\%$ continue to circulate within the plume. The obtained results can be used in planning marine expeditions and assessing the impact of catastrophic water discharges in rivers on the hydrochemical regime and environmental state of the coastal zone.

Keywords: coastal zone, river plume, marine shelf, continental runoff, hydrofront, numerical modeling, Danube, Black Sea, water circulation

Acknowledgments: The study was carried out within the framework of state assignment of FSBSI FRC MHI on theme FNNN-2024-0016.

For citation: Tsyganova, M.V, Lemeshko, E.M, Fomin, V.V. and Ryabtsev, Yu.N., 2025. Modeling of River Plume Propagation in the Coastal Zone of Non-Tidal Sea. *Physical Oceanography*, 32(5), pp. 668-689.

- © 2025, M. V. Tsyganova, E. M. Lemeshko, V. V. Fomin, Yu. N. Ryabtsev
- © 2025, Physical Oceanography

668 ISSN 1573-160X PHYSICAL OCEANOGRAPHY VOL. 32 ISS. 5 (2025)



Introduction

River runoff is the main source of freshwater influx into the seas, containing dissolved substances, suspended matters and products of anthropogenic activity of continental origin, many of which have a negative impact on marine ecology. In the area where river waters flow into the sea, a plume (a freshened water mass formed by the mixing of river runoff and saline marine waters) and an alongshore buoyancy-driven current are formed, which, in turn, influence dynamic processes in the coastal zone. Therefore, studying the spread of river waters on marine shelves is an important fundamental and applied investigation [1–4]. River plumes formed in coastal marine areas in many regions of the world are typically have large square but form a thin surface layer of the sea, which, due to the density gradient, is distinct from the underlying marine waters [4, 5].

The study of the formation and evolution of river plumes is based on the analysis of *in situ* and satellite measurements [5–11], laboratory experiments [12, 13] and numerical modeling [13–18]. Shelf water dynamics are determined by processes of various spatiotemporal scales, such as geostrophic currents, frontal zones, water mass mixing, upwelling/downwelling, wave phenomena and tides. In turn, the formation of a river plume and the associated alongshore buoyancy-driven current depends on numerous factors: estuary geometry, bottom topography, characteristics of the river runoff, the Coriolis parameter, wind forcing, tides and bottom friction. These processes also influence on coastal shelf water dynamics [6–10].

In the absence of external forcing (wind, tides), river waters form a lens of freshened water bounded by a front. For the region considered, its boundary is identified by the 16 PSU isohaline [11]. The characteristic scales of the lens, as the plume core (its width and depth), are determined by the density of the river and shelf waters, the Coriolis parameter and the inflow velocity of the river, which is calculated from the water runoff, width and depth of the estuary [7, 8, 12]. Depending on the characteristic scales of the plume and the bottom topography, different types of plumes are distinguished: bottom-attached, intermediate and surface [9]. This paper considers the surface plume type.

For the Black Sea, in the absence of tidal mixing and for wind forcing less than 5 m/s, the surface plume of rivers such as the Danube and Dniester acquires the characteristic form of a "free plume." It consists of a lens of freshened water in the near-estuary area, bounded by a front, which represents the bulge, and an alongshore current. In a quasi-steady state, the bulge is an anticyclonic eddy, which is due to a cyclostrophic balance [9, 13]. The alongshore current develops in the anticyclonic direction from the estuary as a quasi-geostrophic compensation current [10]. The free plume serves as an ideal object for validating numerical models and estimating plume scales based on *in situ* and remote measurement data under weak wind conditions [14–17]. Based on numerical modeling on seasonal scales, the presence of an anticyclonic eddy in the Danube delta region, formed as a result of the spring flood of rivers in the absence of wind forcing, was established

[18]. Then, taking into account the seasonal variability of river runoff and the wind field, numerical modeling produced maps of the spatial distribution of low-salinity waters from river estuaries in the coastal areas of the Black Sea northwestern shelf (BSNWS) [14]. The combination of these factors with the influence of bottom topography allowed for modeling the characteristic pathways of freshened water spreading on the BSNWS on seasonal [19] and interannual scales [17].

Although the cited studies demonstrate the significant influence of wind on the pathways of river water spreading on the BSNWS, buoyancy, mixing and inertial processes play an important role in the early stages of plume and alongshore current formation. These processes determine the transport of freshened waters and, consequently, suspended and dissolved substances in the coastal shelf zone [15, 20]. In this regard, the mechanisms of bulge formation and the establishment of a quasisteady alongshore current require clarification; quantitative assessments of the redistribution of river water between the plume and the current depending on the hydrological characteristics of the BSNWS waters are needed, as well as parameterization of the plume radius based on its vorticity and depth.

Thus, the purpose of this work is to investigate the propagation of river waters as they flow into the sea, the formation of a plume and coastal buoyancy current as well as to assess the plume characteristics and their evolution parameters, depending on river discharge and hydrological conditions of the BSNWS in the absence of wind and tidal forcing.

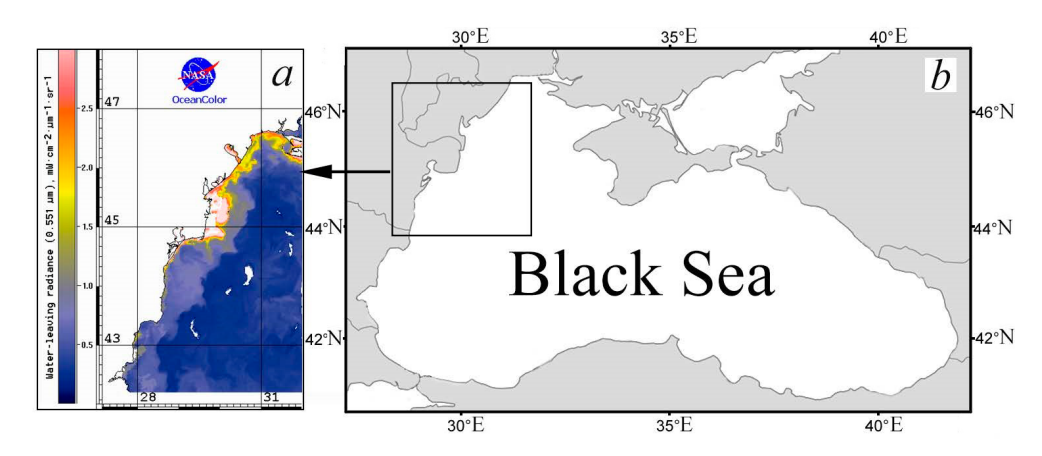
Research area

The BSNWS is characterized by an extensive, shallow shelf. The 50 m isobath is located 50–200 kilometers from the coastline. About 80% of the total river runoff into the Black Sea originates from the Dnieper, Southern Bug, Dniester and Danube rivers, which flow into the shelf waters [21]. The hydrological structure of the area's waters is strongly influenced by wind patterns, winter cooling, summer heating of coastal areas and river runoff fluctuations [21, 22].

The largest river flowing into the Black Sea is the Danube, the second largest river in Europe, with a long-term average annual discharge of 200 km³, accounting for 57.5% of the total river inflow into the Black Sea, and a sediment load reaching 30 million m³ considering regulation [23]. The Danube waters form an extensive plume and a well-developed coastal current (Fig. 1), which also significantly influence the ecological state of the shelf waters and the seasonal cycle of chlorophyll *a* concentration [24].

The horizontal and vertical scales of the plume and the magnitude of the coastal current transport depend on the seasonal cycle of river runoff, the density of the incoming river water and shelf waters, the Coriolis parameter and the estuary geometry. The seasonal variability of river runoff is significant: the maximum discharge for 1985–2006 for the Danube (9530 m³/s) occurs in April and for the Dnieper (1798 m³/s) in May, while the minimum is for the Danube (4700 m³/s) in September and for the Dnieper (724 m³/s) in August [23]. The Danube has an

extensive delta but the main inflow of water into the sea occurs through three primary distributaries: the Kiliya branch (up to 63% of the total discharge), the Sulina branch (17%) and the St. George branch (20%) [25].



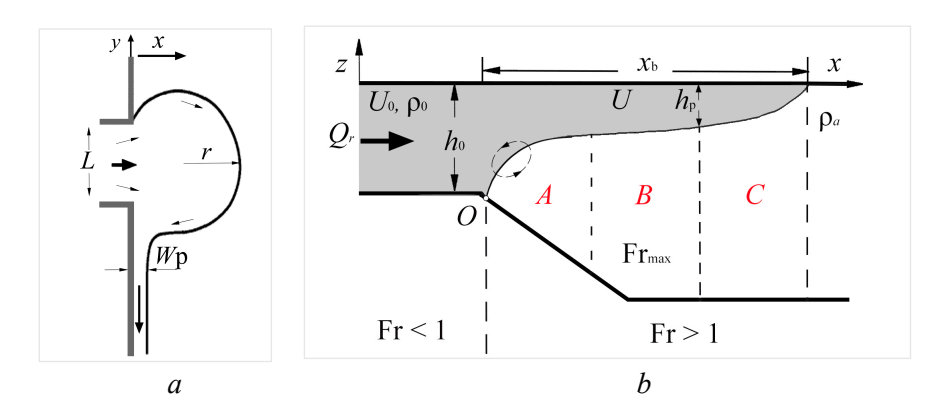
F i g. 1. Enlarged image of the study area (a) with a plume in the Danube Delta region on 01.04.2017 based on satellite data (wavelength 0.551 μ m) (http://dvs.net.ru/mp); Black Sea region (b), the study area is outlined by a rectangular circuit

Data used and research methods

The structure of a river plume includes a source of freshwater with a discharge Q_r , the river mouth width L and the depth h_0 and a transit area of river waters. The mixing zone of river and sea waters includes a plume, formed as a result of the spreading of river waters in the form of an anticyclonic circulation (in the Northern Hemisphere) with the radius r and an alongshore buoyancy-driven current with the width W_p (Fig. 2). For the BSNWS conditions and the Danube River discharge, the inner boundary of the mixing zone of river and sea waters is generally located at a distance of 0–4 km from the river mouth, which approximately corresponds to the inertial scale $L_0 = U_0 f$, where U_0 is the river inflow velocity; f is the Coriolis parameter. The outer boundary of the mixing zone is determined by the position of the inflection point on the salinity profile, beyond which the salinity gradient decreases and its value approaches the background salinity of the shelf waters. For the BSNWS, the water salinity at the outer boundary of the mixing zone is $\sim 16 \, \text{PSU}$, which corresponds to $\sim 90\%$ of the salinity of the open Black Sea waters [11].

Freshwater flows onto the shelf with a velocity determined by the river runoff and the mouth geometry, $U_0 = Q_r/h_0L$ ((Fig. 2), provided that the river flows into the sea at a right angle and is characterized by a hydrodynamic regime with Froude number $Fr = U_0/C_0$, where $C_0 = (g'h_0)^{1/2}$ is phase speed of the gravity wave; $g' = g(\rho_0 - \rho_a)/\rho_0$ is reduced acceleration due to gravity; ρ_0 , ρ_a are densities of river and sea water, respectively. Cases where a river forms an estuary connected to the sea are not considered in this work.

Near the river mouth (near-field plume region), Fr < 1 typically holds, and the plume dynamics are determined by inertia and stratification. At the liftoff point (O), where Fr = 1, the plume detaches from the bottom and spreads in the surface layer with a thickness h_p . This is the flow acceleration zone and the zone of intense mixing due to shear instability and large-scale mixing processes (Zone A). This is followed by Zone B – the flow region with maximum Fr, values exceeding 1, where intensive mixing occurs during the plume propagation. The evolution concludes with Zone C, the area of plume spreading and a gradual decrease in the Froude number down to the outer marine boundary (Fig. 2). Table 1 presents the characteristics of river plumes for different rivers and shelf types obtained from hydrological data [15, 16, 26–27].



F i g. 2. Schematic diagram of formation of plume and water circulation in the river mouth: a – top view; b – frontal section. Designations: L – mouth width; r – plume radius; r – coastal current width; r – river runoff; r – mouth depth; r – river inflow velocity; r – river water density; r – plume width; r – plume velocity; r – plume depth; r – seawater density; r – liftoff point of plume detachment from the bottom at r – 1; r – area of flow acceleration and intense mixing, r – area of intense flow mixing, r – area of plume spread

Table 1

Characteristics of river plumes

Name of the river	$Q_{\rm r}$	$h_{ m p}$	H_{R}	$W_{ m sh}$	$\alpha \times 10^{-3}$	R_{di}	Source
Delaware	650	8.68	14	120	0.7	6.37	[16]
Colombia Mississippi	7500	6.32	30 40 3.6		3.6	8.21	[26]
	19000	10.00	20	200	1.0	12.00	[27]
Danube	6700	15.00	25	50-200	3.0	12.10	[15]

N o t e. Designations: Q_r is river discharge, m³/s; h_p is plume thickness, m; H_R is bottom depth, m, for $x = R_{di}$; W_{sh} is shelf width, km; α is bottom slope; R_{di} is baroclinic Rossby radius, km.

The ratio of the plume thickness h_p to the bottom depth H_R at a distance from the shore equal to the baroclinic Rossby radius R_d , characterizes the plume type: when $h_p/H_R < 1$ the plume is surface-advected, when $h_p/H_R > 1$ it is bottom-advected, and when $h_p/H_R = 1$ the plume is of an intermediate type [16]. The rivers presented in Table 1 form surface-advected plumes and the Danube plume is comparable in parameters, for example, to the Mississippi plume. It should be noted that for the Black Sea, the g' value is on average larger than that for the ocean shelf at the same latitude, which leads to larger horizontal and smaller vertical scales of the plume for the same river discharges.

The horizontal scale and depth of the plume depend on the stratification of the shelf waters and the river water discharge, the seasonal variability of which affects the internal Rossby radius R_d : the difference in R_d values between July and January reaches 2.5 km for the BSNWS [25]. R_d reaches its maximum value in summer: 20 km in the deep part of the sea, up to 12.5 km on the BSNWS, while on the shelf with depths less than 100 m, it ranges from 3.0 to 7.5 km and tends to decrease with increasing latitude [25].

The surface-advected plume and the coastal current are in geostrophic balance with the cross-shelf pressure gradient. This balance is established after two to three inertial periods following the inflow of river water. Accordingly, the plume thickness can be expressed using geostrophic relationships as follows:

$$h_{\rm p} = (2Q_r f/g')^{1/2},$$
 (1)

the baroclinic Rossby radius, taking into account expression (1), in this case is given by [13]:

$$R_{\rm d} = (2Q_r {\rm g}'/f^3)^{1/4}.$$
 (2)

Thus, alongside the inertial scale L_0 and the baroclinic Rossby radius, we will consider the characteristic scale of the depth of the plume lower boundary h_p for investigating the plume structure.

In the surface plume model, when diffusive processes are neglected, its thickness gradually decreases from the value at the mouth to zero at the outer boundary of the anticyclonic eddy, which is in cyclostrophic balance. For this eddy, a relationship is known that allows for the determination of the maximum distance x_b of the surface plume outer boundary from the shore (Fig. 2) based solely on the values of river runoff, channel geometry and the density of river and shelf waters:

$$x_{\rm b} = 2r = \frac{2(3g'h_0 + U_0^2)}{f(2g'h_0 + U_0^2)^{1/2}} = R_{di} \frac{2(3 + Fr_i^2)}{(2 + Fr_i^2)^{1/2}},$$
(3)

where h_0 is mouth depth; U_0 is river inflow velocity; $R_{di} = (g' \cdot h_0)^{1/2} / f$ is baroclinic Rossby radius and the Froude number Fr_i for the inflow [9].

According to equation (3), three cases of plume propagation can be considered, depending on the water inflow velocity from the river arm and the density difference between river and shelf waters. In the case of low inflow velocities or a large density difference, when $u^2 \ll g'h_0$ (which corresponds to a Froude number $Fr_i \ll 1$), it PHYSICAL OCEANOGRAPHY VOL. 32 ISS. 5 (2025)

follows from equation (3) that: $x_b \sim 4.2 R_{di}$. Thus, the outer boundary of the surface plume is located at a distance of approximately four baroclinic Rossby radii from the shore. For example, for the Danube, this distance is $x_b \sim 51$ km; in the area where the shelf is narrowest, the plume reaches its boundary (Table 1, Fig. 1), which agrees with observational results [15]. In terms of length scales, this case, for which the Froude number $Fr_i = L_0/R_{di} \ll 1$, is described as the predominance of the baroclinic Rossby radius over the inertial scale. The river inflow velocity, mouth depth and width also determine the shape of the outflow plume and the coastal buoyancy-driven current through the Rossby number Ro = $U_0/fL = L_0/L$, which describes the influence of inertia and nonlinearity, and the Burger number Bu = R_{di}/L , which characterizes the influence of buoyancy forces. Note that the Froude number can also be expressed as their ratio $Fr_i = Ro/Bu$. In this case, the influence of buoyancy forces, due to the river discharge, exceeds the influence of flow inertia. If the Rossby number Ro < 1, that is, the ratio of the inertial scale to the river mouth width is less than one, the plume has a semicircular shape, is pressed against the shore, and a coastal current is formed, the discharge of which is proportional to the exponential function of Ro [28].

The second limiting case corresponds to high inflow velocities and a small density difference $U^2 >> g'h_0$, which leads to a supercritical regime of plume propagation with a Froude number Fr >> 1, i.e. Ro >> Bu and the plume width is equal to twice the inertial scale: $x_b \sim 2U_0/f = 2L_0$ [28]. The value Fr ~ 1 (or Ro \sim Bu) corresponds to an intermediate regime, the dynamics of which combine features of both limiting cases.

Comprehensive expeditionary studies specifically aimed at investigating the formation and evolution of the Danube plume have not been conducted. The existing data are mainly represented by disparate multi-year measurements of hydrological, hydro-optical and hydrochemical parameters [3, 15, 29]. Analysis of hydrological data indicates that the horizontal size of the plume varies from 28 to 120 km and its thickness varies from 8 to 15 m (according to the 16 PSU isohaline) [15, 29]. When the plume size is about 90 km, it occupies a large area of the shelf; its seaward boundary reaches the 50-75 m isobaths, which influences the hydrological structure and ecological state of the shelf waters. The plume characteristics are significantly influenced by wind conditions. For instance, the anomalous southward propagation of the alongshore buoyancy-driven current recorded in July 1992 was associated with a prolonged strengthening of the northerly wind of up to 10 m/s during the period from July 12 to 18 [15]. On the other hand, the stretching of the plume in the northeastern direction over 120 km on September 2–6, 2004, was caused by the impact of southerly winds with speeds of up to 10 m/s [29]. Thus, the variability of river runoff and the wind field creates diverse conditions for plume formation, which, along with the hydrological conditions of the shelf and the absence of tides, makes the BSNWS a unique testing ground for studying plume dynamics.

Numerical experiments with a three-dimensional hydrodynamic model

This work investigated plume formation and propagation using numerical modeling with the three-dimensional sigma-coordinate Princeton Ocean Model (POM), designed for calculating circulation in coastal zones accounting for river runoff [30–32]. Sigma-coordinate models are widely used for modeling dynamic processes in shallow waters because the automatic clustering of sigma-levels with decreasing basin depth allows for high vertical resolution. Furthermore, these models ensure the precise satisfaction of kinematic boundary conditions at the free surface and the bottom [31].

Calculations were performed for a rectangular domain. The coordinates of the computational domain are $29.5^{\circ}-31.5^{\circ}E$, $43.35^{\circ}-45.75^{\circ}N$. The number of grid nodes is 51 along the *x*-axis and 171 along the *y*-axis. At the initial time, the model specifies the inflow of freshened water through the river mouth with a defined discharge and salinity.

The flux of river water, in the absence of wind and tides, propagates seaward and then, under the influence of the Coriolis force, turns in an anticyclonic direction (in the Northern Hemisphere) [9, 31]. As a result, an outflow water forms bulge in the near-field plume zone, and after approximately two inertial periods, a buoyancy-driven alongshore jet current is established (Fig. 2). In general, a plume is a non-stationary formation, and one of the factors stabilizing its dynamics is a steady background current directed southward along the propagation path of the alongshore jet of freshened waters [30–32].

The model is based on the three-dimensional circulation equations in the σ -coordinate system $\sigma = (z - \eta)/H$, $\sigma \in [0, 1]$, where x, y, z are Cartesian coordinates; $H = h + \eta$ is sea depth; h(x, y) is sea bottom topography; $\eta(x, y, t)$ is sea surface elevation. The dynamics of frontal zones are described using the primitive equations of motion for a continuously stratified, viscous, incompressible fluid under the Boussinesq and hydrostatic approximations, which have the following form:

$$\frac{\partial uH}{\partial t} + gH\frac{\partial \eta}{\partial x} - fvH + \frac{H}{\rho_0}\frac{\partial p}{\partial x} = \frac{\partial}{\partial \sigma} \left[\frac{K_M}{H} \left(\frac{\partial u}{\partial \sigma} \right) \right] + HF_X + G_X, \tag{4}$$

$$\frac{\partial vH}{\partial t} + gH\frac{\partial \eta}{\partial y} + fuH + \frac{H}{\rho_0}\frac{\partial p}{\partial y} = \frac{\partial}{\partial \sigma} \left[\frac{K_M}{H} \left(\frac{\partial v}{\partial \sigma} \right) \right] + HF_Y + G_Y, \tag{5}$$

$$\frac{\partial \eta}{\partial t} + \frac{\partial uH}{\partial x} + \frac{\partial vH}{\partial y} + \frac{\partial w}{\partial \sigma} = 0, \tag{6}$$

$$\frac{\partial TH}{\partial t} + \Lambda T = \frac{\partial}{\partial \sigma} \left[\frac{K_H}{H} \left(\frac{\partial T}{\partial \sigma} \right) \right] + HF_T, \tag{7}$$

$$\frac{\partial SH}{\partial t} + \Lambda S = \frac{\partial}{\partial \sigma} \left[\frac{K_H}{H} \left(\frac{\partial S}{\partial \sigma} \right) \right] + HF_S. \tag{8}$$

where u, v, w are velocity components along x, y, σ , respectively; ρ_0 is mean density; f is Coriolis parameter; T, S are water density and salinity.

The following notation is adopted for the advection operator:

The HF_X , HF_Y , HF_T , HF_S terms parameterize horizontal turbulent viscosity and diffusion and have the following form:

$$HF_{X} = \frac{\partial}{\partial x} \left[2A_{M}H \frac{\partial u}{\partial x} \right] + \frac{\partial}{\partial y} \left[A_{M}H \left(\frac{\partial u}{\partial y} + \frac{\partial v}{\partial x} \right) \right],$$

$$HF_{Y} = \frac{\partial}{\partial x} \left[A_{M}H \left(\frac{\partial u}{\partial y} + \frac{\partial v}{\partial x} \right) \right] + \frac{\partial}{\partial y} \left[2A_{M}H \frac{\partial v}{\partial y} \right],$$

$$HF_{T,S} = \frac{\partial}{\partial x} \left[A_{H}H \frac{\partial (T,S)}{\partial x} \right] + \frac{\partial}{\partial y} \left[A_{H}H \frac{\partial (T,S)}{\partial y} \right].$$

 A_M , A_H depend on the horizontal velocity gradients:

$$(A_M, A_H) = \frac{\delta}{2} (C_M, C_H) a^{1/2}, \quad a = \left(\frac{\partial u}{\partial x}\right)^2 + \left(\frac{\partial v}{\partial y}\right)^2 + \frac{1}{2} \left(\frac{\partial u}{\partial y} + \frac{\partial v}{\partial x}\right)^2,$$

Where C_M , C_H and δ are some constants.

The coefficients of vertical turbulent viscosity and diffusion are determined by the equations: $K_M = \max(LqS_M, K_{M\varphi})$, $K_H = \max(LqS_H, K_{H\varphi})$, where $q^2/2$ is turbulent kinetic energy; L is turbulence macroscale; S_M , S_H are functions of the dynamic Richardson number; constants $K_{M\varphi}$, $K_{H\varphi}$ are background values. The functions q, L are found from the solution of the turbulent energy balance equations solved together with the main problem.

The following boundary conditions are applied at the surface and bottom:

$$\sigma = 0 \quad w = 0, \quad \frac{K_M}{H} \left(\frac{\partial u}{\partial \sigma}, \frac{\partial v}{\partial \sigma} \right) = \frac{1}{\rho_0} \left(\tau_X^0, \tau_Y^0 \right), \quad \frac{K_H}{H} \left(\frac{\partial T}{\partial \sigma}, \frac{\partial S}{\partial \sigma} \right) = \frac{1}{\rho_0} \left(Q_T, Q_S \right), \quad (9)$$

$$\sigma = -1 \quad w = 0, \quad \frac{K_M}{H} \left(\frac{\partial u}{\partial \sigma}, \frac{\partial v}{\partial \sigma} \right) = \frac{1}{\rho_0} \left(\tau_X^B, \tau_Y^B \right), \quad \frac{K_H}{H} \left(\frac{\partial T}{\partial \sigma}, \frac{\partial S}{\partial \sigma} \right) = 0,$$

where Q_T , Q_S are heat and salt fluxes. Expressions for the tangential stresses at the free surface and bottom respectively are as follows: $(\tau_X^0, \tau_Y^0) = \rho_a C_A |W|(w_X, w_Y), \quad (\tau_X^B, \tau_Y^B) = \rho_a C_D |U|(u, v), \text{ where } \rho_a \text{ is air density; } C_A,$ C_D are friction coefficients; $W = (w_X, w_Y)$ is wind speed at 10 m height; U = (u, v) is horizontal current velocity.

At solid lateral boundaries, velocities, heat and salt fluxes are set to zero.

Spatial discretization of the equations is performed on a C-grid. Uniform steps in the x-, y- and σ -coordinates are used. The evolutionary equations are integrated in time with a step Δt using the time-splitting method.

The horizontal velocity U is represented as the sum of a depth-independent component of \overline{U} barotropic and U' baroclinic components:

$$U = \overline{U}(x, y, t) + U'(x, y, \sigma, t).$$

An overbar denotes the result of integration over the σ -coordinate from -1 to 0. Integrating equations (4)–(6) vertically using boundary conditions (9) yields a system of shallow-water equations for determining the barotropic velocity components and sea level:

$$\frac{\partial \overline{u}H}{\partial t} + gH\frac{\partial \eta}{\partial x} - f\overline{v}H + \frac{H}{\rho_0}\frac{\partial p}{\partial x} = \frac{1}{\rho_0}(\tau_X^0 - \tau_X^B) + H\overline{F}_X + \overline{G}_X, \tag{10}$$

$$\frac{\partial \overline{v}H}{\partial t} + gH\frac{\partial \eta}{\partial y} - f\overline{u}H + \frac{H}{\rho_0}\frac{\partial p}{\partial y} = \frac{1}{\rho_0}(\tau_Y^0 - \tau_Y^B) + H\overline{F}_Y + \overline{G}_Y, \tag{11}$$

$$\frac{\partial \eta}{\partial t} + \frac{\partial \overline{u}H}{\partial x} + \frac{\partial \overline{v}H}{\partial y} = 0. \tag{12}$$

The equations for the baroclinic velocity components have the following form:

$$\frac{\partial u'H}{\partial t} - fv'H = \frac{\partial}{\partial \sigma} \left[\frac{A_M}{H} \left(\frac{\partial u'}{\partial \sigma} \right) \right] - \frac{1}{\rho_0} (\tau_X^0 - \tau_X^B) + H(F_X - \overline{F}_X) + G_X - \overline{G}_X, \tag{13}$$

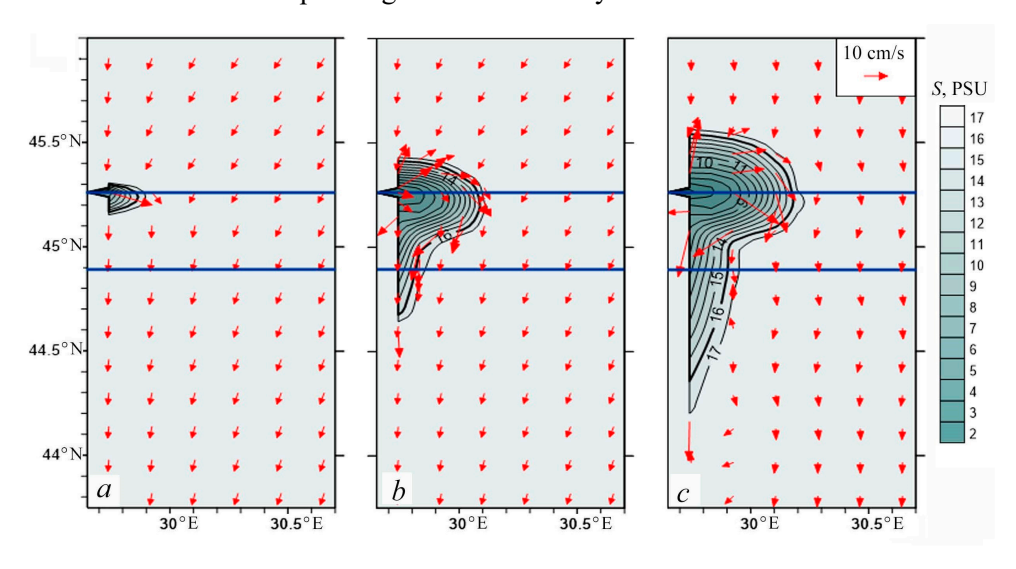
$$\frac{\partial v'H}{\partial t} - fu'H = \frac{\partial}{\partial \sigma} \left[\frac{A_M}{H} \left(\frac{\partial v'}{\partial \sigma} \right) \right] - \frac{1}{\rho_0} (\tau_Y^0 - \tau_Y^B) + H(F_Y - \overline{F}_Y) + G_Y - \overline{G}_Y, \quad (14)$$

Equations (10)–(12) and (13)–(14) are approximated by explicit schemes. Furthermore, a small-time step $\Delta t_A = \Delta t/n$ is used in the barotropic problem, where n is chosen according to the Courant stability criterion. When solving the heat and salt transport equations (7)–(8), the three-dimensional transport and horizontal diffusion along the vertical coordinate is separately identified and solved using the Thomas algorithm (tridiagonal matrix algorithm) taking into account the boundary conditions (9).

The numerical algorithm of the model is based on splitting the task into barotropic and baroclinic modes and applying explicit schemes for the horizontal

coordinates and implicit schemes for the σ-coordinate. The advective operator in the model equations is approximated by TVD schemes [31], which ensure the monotonicity of the numerical solution, necessary for the correct description of fields with large spatial gradients. Furthermore, a recent study on the influence of various numerical schemes on salt diffusion calculations showed that using TVD schemes significantly reduces computational viscosity, leading to less distortion of the plume dynamics compared to other difference schemes [33].

Rectangular domain. A rectangular basin of constant depth of 40 m with the coordinates specified above was used in the calculations; the bottom slope near the shore ranges from 3×10^{-3} to 0.6×10^{-4} . The origin of the coordinate system is located at the free surface in the lower left corner of the computational domain. The western model boundary corresponds to the coastline, while the other three boundaries are open. The source of river runoff is located at the grid node with coordinates x = 2, y = 106 and is characterized by a water discharge Q_r ranging from 1500 to 8000 m³/s. The closing cross-section of the river mouth has a width L = 1570 m and a depth $h_0 = 8$ m (Fig. 2). At the initial time, the water salinity in the basin was $S_f = 18$ PSU and the salinity of the incoming water varied from 2 to 6 PSU, which corresponds to values at the inner boundary of the river and seawater mixing zone [11]. The influence of the source is superimposed on a background meridional steady current vo, which, at the initial time, had a velocity ranging from 5 to 25 cm/s and was directed southward. At the opened boundaries of the computational domain, smooth continuation conditions [30, 31] were specified for the current velocity components and salinity assuming equality to zero of the normal derivative from the desired probabilistic variable $\partial \varphi / \partial n = 0$, where n is the normal to the corresponding domain boundary.



F i g. 3. Surface salinity field for river runoff ($Q_r = 1500 \text{ m}^3/\text{s}$, salinity is 2 PSU) under no wind and at the Rossby number Ro = 0.75: a – after 1 day; b – after 5 days (current discharge in the plume through section CD $Q_{\text{fcc}} = 107 \text{ m}^3/\text{s}$); c – after 10 days ($Q_{\text{fcc}} = 251 \text{ m}^3/\text{s}$). Arrows indicate current velocity; AB, CD – sections by latitude; initial background current velocity is 5 cm/s

The modeling was conducted for a period of 10–30 days on a horizontal grid with $\Delta x = 3137$ m and $\Delta y = 1570$ m. For more detailed resolution in the vertical coordinate, 25 non-uniform levels were used, clustered near the free surface. The horizontal turbulent viscosity coefficient was calculated using the Smagorinsky equation [30, 31]. The vertical viscosity and diffusion coefficients were determined using the Mellor–Yamada method [30, 31]. The baroclinic component of the model was integrated with a time step of 2 minutes and the barotropic component was integrated with a time step of 6 seconds. The numerical solution establishment was monitored based on the values of kinetic energy and water discharge in the cross-sections indicated in Fig. 3.

Results and discussion

The following parameters were specified for modeling the plume: mouth width L=1570 m, mouth depth $h_0=8$ m, river discharge Q_r in the range of 1500–8000 m³/s; for river waters – salinity S in the range of 2–6 PSU, temperature T=15 °C; for shelf waters – salinity S = 18 PSU, T=15 °C; the density of river water ρ_0 and sea water ρ_a was calculated from the equation of state for the given salinity and temperature values; Coriolis parameter f=0.0001013 s⁻¹, inertial period $T_0=2\pi/f=17$ h.

For this model configuration, calculations were performed that demonstrate the formation and propagation of the plume in the absence of wind and the influence of shelf water stratification. Fig. 3 shows the surface salinity distribution after 1, 5 and 10 days for run 1 (Table 2) of the calculation with depth-uniform stratification, with a water discharge Q of 1500 m³/s and river water salinity of 2 PSU. The Rossby number Ro = 0.75 and the Burger number Bu = 6.13 characterize the influence of buoyancy forces. The Froude number $Fr_i = Ro/Bu = 0.13$ (Table 2) indicates that the buoyancy forces due to the river discharge dominate over the inertial forces of the flow; therefore, the plume is pressed against the shore. Since the Rossby number Ro < 1, meaning the ratio of the inertial scale to the river mouth width is less than one, the plume has a semicircular shape, is pressed against the shore, and a current develops along the coast (Fig. 3, a).

Characteristics of plume and depth h_p according to equation (2)

Calcula	ted data	Fr	L ₀ , km	h _p , m	H _p , m	Hcc, m	R _{di} , km	R _p , km	$R_{\rm p}/R_{di}$	Xc/Rp	$H_{ m p}/h_{ m p}$
S, PSU	Q, m ³ /s	LI									
2	1500	0.13	1.2	1.6	5.0	3.2	9.6	22.8	2.4	0.2	3.1
2	3000	0.25	2.2	2.3	6.5	4.0	9.6	21.3	2.2	0.6	2.9
2	8000	0.65	6.3	3.7	10.5	6.8	9.6	24.4	2.5	0.5	2.8
6	3000	0.28	2.4	2.6	6.3	4.1	8.3	22.8	2.7	0.4	2.4
6	8000	0.76	6.3	4.3	11.0	6.7	8.3	24.4	2.9	0.5	2.6

N o t e. Model values are given for t = 10 days. Designations: X_c is latitudinal displacement of plume center from the coast; H_p is plume depth at its center; H_{cc} is its depth near the coast at section CD. The depths H_p and H_{cc} are determined from the position of the 16 PSU isohaline.

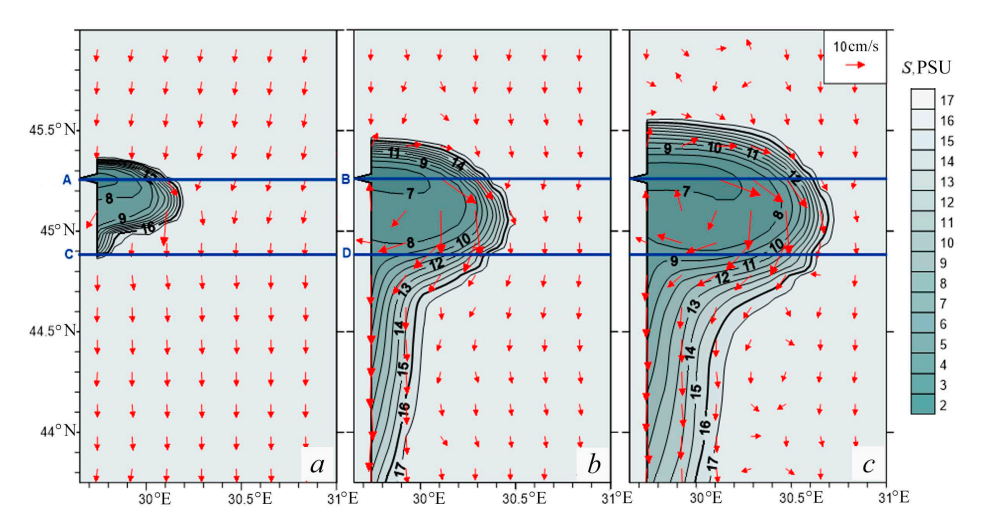
Table 2

During the initial period (after 1 day), a rounded plume forms under the influence of the freshwater discharge from the source. Cross-section AB passes through the estuary along the latitude, while CD is located approximately 31 km south of AB (Fig. 3, a). Within 1.5–2 inertial periods T_0 , under the influence of the Coriolis force, an alongshore current begins to form from the mouth in an anticyclonic direction, which subsequently propagates southward along the western boundary (Fig. 3, b, c). After 3.25 days, the leading edge of the front, identified by the 16 PSU isohaline, reaches cross-section CD (Fig. 3). By day 5, a coastal buoyancy-driven current forms, transporting part of the water from the anticyclonic circular eddy region southward (Fig. 3, b). Meanwhile, the majority of the river water remains within the plume area, leading to an increase in its depth H_p and width up to two radii $2R_p$ (Fig. 3, c).

By day 10, the plume depth H_p reaches 5 m and the plume radius R_p reaches 22.8 km. This plume growth leads to the displacement of its center from the shore seaward by a distance X_c , but no plume detachment from the shore occurs, as its position stabilizes by day 10: $X_c/R_p = 0.2$ (Table 2), and its radius reaches a quasisteady value.

An increase in water discharge with the same estuary dimensions increases the river inflow velocity, leading to higher Froude and Rossby numbers. With a high river inflow velocity and a narrow mouth width (Ro_i > 1), the plume assumes a more rounded shape, while the propagation speed of the buoyancy-driven coastal current front southward increases. The dependence of the plume shape and the intensity of the coastal current on the Rossby number is also noted from in situ observations [29]. An increase in the density of the incoming water (in these numerical experiments, achieved by increasing the river salinity) leads to a decrease in the reduced gravity g', which, according to equation (2), increases the plume depth and the Froude number but reduces the role of stratification via the Rossby radius (equation (3)) and the Burger number. The balance between buoyancy and inertial forces is determined by the combination of river discharge and its density (salinity), which influence the plume depth h_p and its radius r, the plume center position and the regime of the density-driven current formation. Various calculation scenarios are presented in Table 2. For comparison with the plume shown in Fig. 3, consider run 5 (Table 2) with a river discharge $Q_r = 8000 \text{ m}^3/\text{s}$ and salinity S = 6 PSU (Fig. 4). This regime is characterized by larger values of Ro = 4, Fr = 0.76, inertial scale L_0 = 6.3 km, but smaller Burger number Bu = 5.31 and Rossby radius R_{di} = 8.3 km (Table 2). Although the value Fr = 0.76 remains below the critical value, it is almost six times greater than Fr = 0.12 for run 1 (Fig. 3). Thus, the influence of flow inertia has increased sixfold compared to the influence of buoyancy forces. As a result, the plume is elongated from the shore toward the shelf, with its center displaced seaward. However, no detachment of the plume from the shore occurs, as the relative displacement is $X_c/R_p = 0.5$ (Fig. 4, c).

Since in this calculation the Rossby number Ro = 4 (exceeds 1), meaning the inertial scale is four times the mouth width. Thus, the plume forms within 1.5 inertial periods T_0 and has a more circular shape than in Fig. 3, a. The leading edge of the alongshore current front reaches cross-section CD after 1 day (Fig. 4). Considering the distance between the cross-sections, the front propagation speed was $C_p \sim 0.29$ m/s. By day 5, a more developed coastal buoyancy-driven current forms (compared to Fig. 3), which transports part of the waters from the plume area across the southern boundary of the domain (Fig. 4, b). Meanwhile, the majority of the river-derived water accumulates in the plume area, leading to an increase in its depth H_p and radius (Fig. 4, b, c). By day 10, the 8 PSU isohaline reaches 30.5° E, the plume depth H_p (determined by the depth of the 16 PSU isohaline) reaches 11 m and the plume radius R_p reaches 24.4 km. This plume growth is accompanied by the displacement of its center from the shore seaward by a distance X_c . After 10 days, its position stabilizes: $X_c/R_p = 0.5$ (Table 2), and the plume radius reaches a stable value.



F i g. 4. Surface salinity field for river runoff under no wind ($Q_r = 8000 \text{ m}^3/\text{s}$, salinity is 6 PSU) at the Rossby number Ro = 4: a – after 1 day ($Q_{\text{fcc}} = 25 \text{ m}^3/\text{s}$); b – after 5 days (current discharge in the plume through section CD $Q_{\text{fcc}} = 1592 \text{ m}^3/\text{s}$); c – after 10 days ($Q_{\text{fcc}} = 1920 \text{ m}^3/\text{s}$); arrows indicate current velocity; AB, CD – sections by latitude; initial background current velocity is 5 cm/s

An understanding of the plume vertical structure is provided by the salinity cross-sections AB in Fig. 5. The river salinity S is the same in both cases – 6 PSU; only the discharge Q_r differs: 3000 m³/s (Fig. 5, a–c) and 8000 m³/s (Fig. 5, d–f).

Doubling the river discharge for the case where S = 6 PSU, Q = 3000 m³/s leads to an increase in the inflow velocity and, consequently, to an increase in the Rossby (Ro = 4) and Froude (Fr = 0.76) numbers. This results in the plume forming in a more elongated shape toward the shelf and the inertial scale increases to 6.3 km (Fig. 5, d–f) compared to 2.4 km in the first case (Fig. 5, a–c). Since the Froude number in

the second case is 2.7 times larger and approaches the critical value, the plume liftoff point from the bottom shifts toward the shelf (Fig. 2) and the accumulation of most of the incoming river water leads to an increase in the plume depth to 11 m compared to 6.3 m in the first case (Fig. 5, c, f). After the formation of the plume and the coastal current within 1.5–3 inertial periods, the velocities are in geostrophic balance with the pressure gradient.

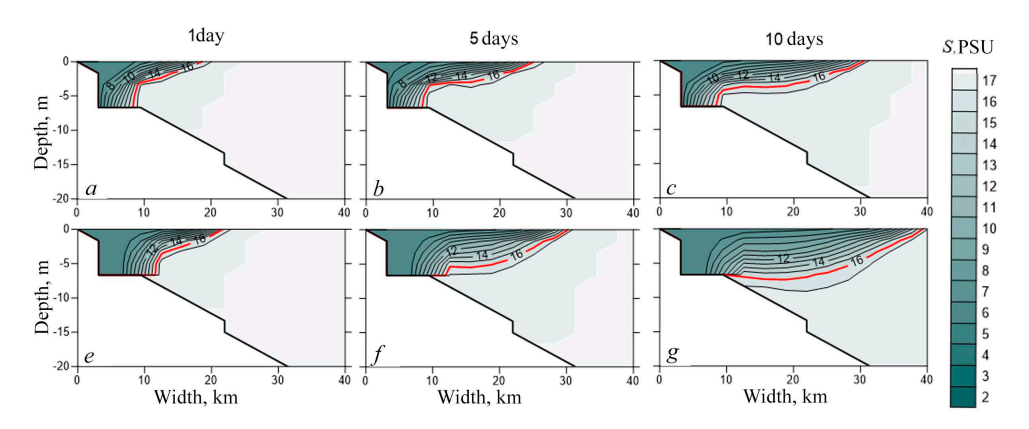
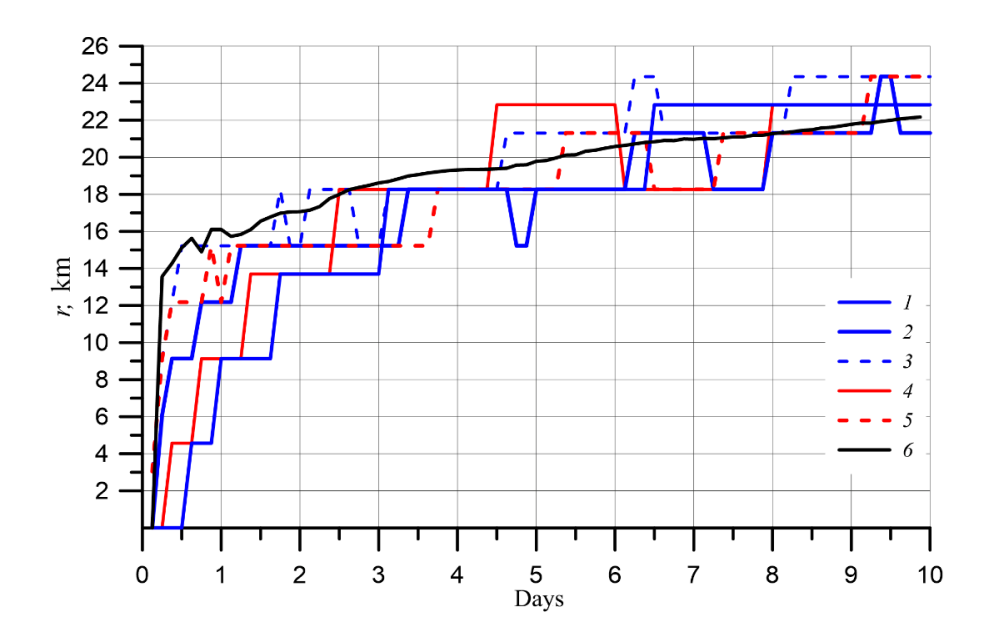


Fig. 5. Zonal sections AB (see Fig. 4) of salinity field after 1, 5 and 10 days (S = 6 PSU) at a discharge Q equal to 3000 m³/s (a, b, c), 8000 m³/s (d, e, f). The 16 PSU isohaline is highlighted in red



F i g. 6. Plume radius obtained from the model data $R_p(t)$ at S = 2 PSU and Q equal to 1500 m³/s (1), 3000 m³/s (2); 8000 m³/s (3); at S = 6 PSU and Q equal to 3000 m³/s (4); 8000 m³/s (5); radius r(t) (6) calculated by equation (15) at S = 2 PSU, Q = 3000 m³/s, ω = -0.8f and $h_{max} = 6.5$ m (Table 2)

Furthermore, the water motion within the bulge can be considered as solid-body rotation, since observations and laboratory experiments show that the vorticity within the bulge is constant and close in magnitude to the Coriolis parameter. Within this assumption, a relationship for the maximum curvature and depth of the plume was derived in [13], allowing for the estimation of its radius depending on the vorticity:

$$r = \left(-\frac{4g' \cdot h_{\text{max}}}{\omega \cdot \left(\frac{\omega}{2} + f\right)}\right)^{\frac{1}{2}},\tag{15}$$

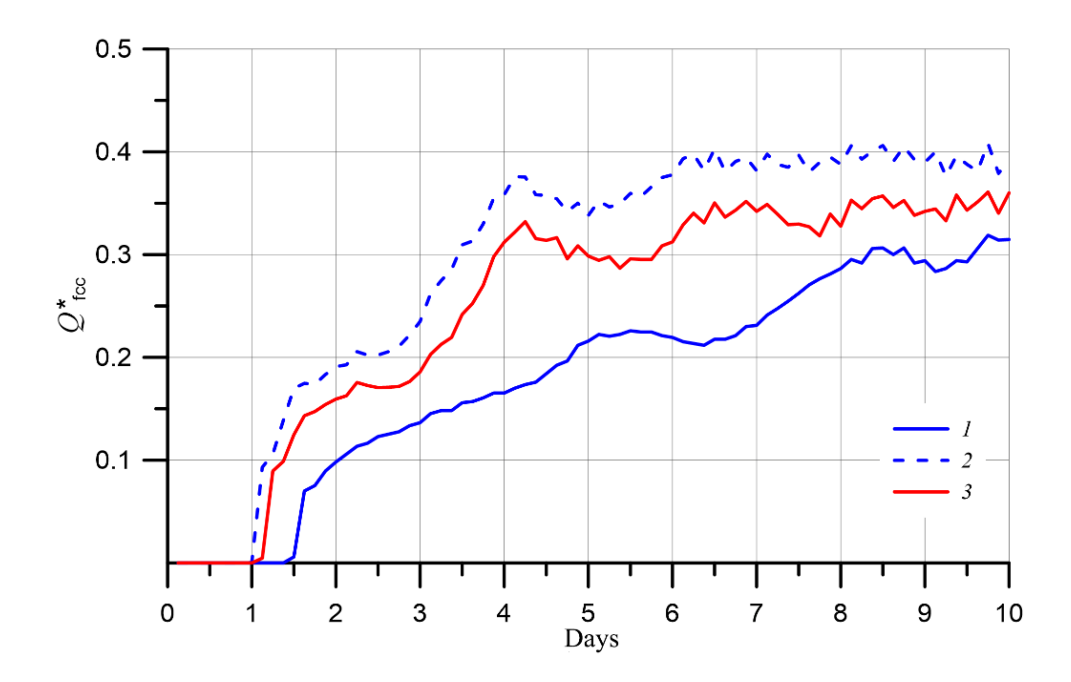
where r is plume radius; h_{max} is its maximum depth; ω is mean vorticity; f is Coriolis parameter; g' is reduced gravity. Based on the modeling results, the plume radius and depth were estimated from the position of the 16 PSU isohaline.

The evolution of the plume radius relative to its center X_c for different experiments is shown in Fig. 6 (Table 2). The mean plume vorticity ω ranged from -0.95f to -0.6f. In all experiments, the plume center moves away from the shore as the Froude number increases; however, no plume detachment from the shore occurs: the ratio X_c to the plume radius increases from 0.2 at a discharge of 1500 m³/s and Fr = 0.13 to 0.5–0.6 at Fr = 0.76, remaining always less than 1 (Table 2). A sharp increase in the plume radius is observed within 1.5–3 inertial periods (Fig. 6). After the coastal current forms and geostrophic balance is established, the radius increases approximately linearly with time and reaches 21–24 km (Fig. 6). The $R_p(t)$ graphs, obtained from the model data, are well approximated by equation (14) with $\omega = -0.8f$ and the maximum plume depth $h_{\text{max}}(t)$, determined from the 16 PSU isohaline. It should be noted that estimating the plume radius using equation (3) underestimates the r values for all variants in Table 2, as it corresponds to a steady state. For all graphs in Fig. 6 Fr < 1 and the ratio of the plume radius to the baroclinic Rossby radius R_{di} is 2.2–2.9, which corresponds to the plume classification based on equation (3) for the case of low inflow velocities and large density differences $u^2 \ll g'h_0$ with a Froude number $Fr_i < 1$ and an estimate of $r \sim 2.1 R_{di}$.

After the establishment of the geostrophic circulation regime in the plume and the advancement of the coastal current front southward, the transport of freshwater Q_{fcc} by this current through the vertical cross-section CD was estimated using equation:

$$Q_{fcc}(t) = \iint_{CD} \frac{\left(S_0 - S(t, x, z)\right)}{S_0} V(t, x, z) dx dz, \tag{16}$$

where $S_0 = 18$ PSU is shelf water salinity; V is meridional velocity component; integration is performed over cross-section CD (see Figs. 3, 4).



F i g. 7. Freshwater transport Q^*_{fcc} through section *CD* based on model data normalized to the river freshwater discharge $Q_{\text{fw}} = (S_a - S_0)/(S_a \cdot Q_r)$, with S = 2 PSU and $Q_r = 3000$ m³/s (1), 8000 m³/s (2); with S = 6 PSU and Q = 8000 m³/s (3)

Considering that the amount of freshwater entering the plume depends on the salinity of the river water in the mouth, we introduce a normalized freshwater transport by the coastal current: $Q^*_{fcc} = Q_{fcc}/(\gamma Q_r)$, where $\gamma = (S_0 - S)/S_0$ is the fraction of freshwater in the river. Graphs of Q^*_{fcc} for various modeling scenarios are shown in Fig. 7. For the same river discharge, the transport of freshwater by the coastal current is greater when the river salinity S is lower (Fig. 7), i.e., it is proportional to the increase in the freshwater fraction γ in the river according to equation (16). For the same salinity (i.e., a fixed value of γ), an increase in river discharge and, accordingly, an increase in the water inflow velocity at the estuary leads to higher velocities within the plume and the coastal current. According to equation (16), this results in an increase in Q^*_{fcc} proportional to the river discharge Q_r (Fig. 7).

Note that after 4–5 days, the time dependence of the freshwater transport for all scenarios becomes nearly linear (Fig. 7). This is because, within this time, the leading edge of the alongshore current front reaches the southern boundary of the computational domain and a quasi-steady plume regime is established (see Figs. 3, 4). The potential energy of the coastal current $E_p = (g' \cdot h)$, calculated from the model data where h is the depth of the current near the shore, shows a temporal dependence similar to Q^*_{fcc} . In [28], for the case of equal temperatures of shelf and river water and a linear dependence of the equation of state on salinity ($\Delta \rho = \beta \cdot \Delta S$) it is shown that the value Q_{fcc} from equation (16) can be estimated as $Q_{\text{fcc}} \approx C \cdot E_p^2 / f$,

where $C = \rho_0/(2 \cdot g \cdot \beta \cdot S_0)$ is a constant. Thus, the freshwater transport depends only on the square of the potential energy of the coastal current.

As the plume develops and its leading front reaches cross-section CD, the discharge Q^*_{fcc} begins to increase over 4–5 days (see Fig. 4), transitioning to a quasi-steady regime by day 10. In this case, the coastal current transport is described by the equation $Q_{\text{fcc}}^* = 1/(1+2\cdot\alpha)$, where $\alpha = -2\cdot U_{\theta}/f \cdot r$ is the mean vorticity of the bulge, normalized by the Coriolis parameter [13], $U_{\theta} = -(18 \cdot Q_{\rm r} \cdot f \cdot g^2)^{1/4}$ is the azimuthal velocity of the plume [33]; r is the plume radius. The value $Q^*_{
m fcc}$ was estimated using the given equations with the plume radius and g' from the model data at time t = 10 days (Table 2), when the Q_{fcc}^* discharges were close to steady (Fig. 7). For the second calculation variant ($\alpha = 0.83$, $Q_{\text{fcc}}^* = 0.38$); the third ($\alpha = 0.93$, $Q_{\text{fcc}}^* = 0.35$) and the fifth ($\alpha = 0.87$, $Q_{\text{fcc}}^* = 0.37$) agreement with the model Q_{fcc}^* values is noted (Fig. 7). Thus, for river discharges from 3000 to 8000 m³/s and river water salinities from 2 to 6 PSU, when the freshwater transport reaches a quasi-steady regime, about 40% of the river water is transported by the coastal current, while about 60% remains circulating in the plume, leading to its expansion and slow growth in depth and radius (Fig. 6). Such a distribution of river discharge has been observed in both laboratory experiments and numerical modeling [10, 13], as well as in the analysis of hydrological data in plume formation areas [13].

A background current, aligned with the direction of propagation of the coastal buoyancy-driven current from the river mouth, stabilizes the plume and accelerates the front movement. When calculations were repeated with a background current velocity of 10 to 25 cm/s, an increase in $Q^*_{\rm fcc}$ and a faster transition to a quasi-steady regime were observed. For example, with a background current velocity $V_{\rm fon} = 25$ cm/s, the $Q^*_{\rm fcc}$ value doubled compared to the scenario with $V_{\rm fon} = 5$ cm/s on day 5 of the calculation. The obtained results are valid not only in the absence of wind forcing but also under weak winds. It is demonstrated in [20] that during plume formation, wind forcing begins to dominate over buoyancy driven by freshwater river inflow at wind speeds greater than 5.7 m/s for an average Danube discharge of 6000 m³/s and typical density values for the BSNWS (reduced gravity $g' \sim 0.02-0.11$ m/s²). Thus, for weak winds (with speeds less than 5 m/s), equations (1) and (15) allow estimating the characteristic depth and horizontal scale of the plume, which can be used in the analysis of *in situ* and satellite data.

Conclusion

Based on numerical modeling using the POM three-dimensional sigmacoordinate model, calculations of circulation in the coastal zone accounting for river discharge were carried out. The formation of the river plume and the coastal buoyancy-driven current under various river discharge rates and shelf water stratification conditions characteristic of the BSNWS were investigated.

The advective operator in the model equations was approximated by TVD schemes, which ensured the monotonicity of the numerical solution in areas with large spatial gradients of hydrophysical parameters. The use of TVD schemes also

significantly reduced computational viscosity, leading to less distortion of the plume dynamics compared to other finite-difference schemes.

Formation and evolution of the plume were modeled for five numerical runs with different river salinity and discharge rates within the Froude number range from 0 to 1. In these cases, buoyancy forces due to river discharge dominate over flow inertia, so the plume remains pressed against the shore. The plume has a semicircular shape. If the Rossby number Ro < 1, meaning the ratio of the inertial scale to the river mouth width is less than one, the plume remains pressed against the shore. The balance between buoyancy forces (Burger number) and inertia (Froude and Rossby numbers) depends on the combination of river discharge and its density (salinity), which influence the plume depth, its radius r, shape, center position and the regime of buoyancy-driven current formation.

At the initial stage (time $t \sim T_0$, where T_0 is the inertial period), an anticyclonic eddy begins to develop near the river mouth. By time $t \sim 2T_{0\,the}$ eddy forms the plume core and, reaching the shore south of the mouth, forms a buoyancy-driven coastal current that transports freshwater southward. After $t \sim 2T_0$ the water circulation in the plume and current obeys a geostrophic balance with the cross-shelf pressure gradient.

The plume consists of a core region, where the azimuthal velocity increases linearly from its center, and an outer region, where velocities are close to zero. This plume structure is confirmed by laboratory experiments and observations and indicates constant vorticity ω in the bulge, with the value $\omega \sim -f$, meaning the potential vorticity is close to zero. The outer seaward boundary of the plume and its depth coincide with the position of the 16 PSU isohaline, and the plume radius R_p calculated using equation (15) considering the maximum plume depth and the mean plume vorticity ω corresponds better to the model R_p values than the steady-state estimate (equation (3)). As the ratio of the inertial scale to the Rossby radius increases, the plume radius also increases and reaches $R_p = 24$ km for the experiment with Fr = 0,76, with the ratio R_p to the Rossby radius reaching 2.9, and the plume center shifts seaward by a distance of 0.5 R_p . The plume depth H_p and coastal current velocity calculated by the model exceed the estimates from equation (1) by a factor of 2.4–3.1; however, the H_p values and plume width $x_b = 2R_p$ agree with hydrological observation data obtained under weak wind conditions (up to \sim 5 m/s).

The propagation speed of the leading edge of the buoyancy-driven coastal current front, according to model estimates, corresponds to the phase speed of gravity-driven current along the shelf slope $C_{\rm p}$ and is $\sim 0.15-0.32$ m/s. The freshwater discharge $Q^*_{\rm fcc}$, transported by the coastal current is proportional to the square of its potential energy. After $t \sim 5T_0$ the dependence of $Q^*_{\rm fcc}$ in the square of the potential energy is described by a linear regression with a coefficient of determination ~ 0.95 and a correlation coefficient ~ 0.97 . After 10 days ($t \sim 10T_0$) a quasi-steady regime is established, in which the coastal current transport constitutes about 40% of the total river discharge, while 60% continues to circulate in the plume, leading to its further expansion.

The obtained relationships for plume depth and width as well as coastal current freshwater transport can be used to estimate these parameters from hydrological information or satellite data at wind speeds less than 5 m/s. The results of the study can be used for planning marine expeditions in coastal zones with river inflow, assessing the impact of catastrophic water discharges or river floods on the hydrochemical regime and ecological state of the coastal zone. The results can also be used for developing methods of satellite data analysis, as the regression relationships established in the study allow estimating the variability of freshwater discharge in the coastal zone Q*fec from satellite measurements.

REFERENCES

- 1. Zavyalov, P. and Makkaveev, P., 2014. River Plumes in Sochi Water Area. *Science in Russia*, (2), pp. 4-12 (in Russian).
- Osadchiev, A., Sedakov, R. and Barymova, A., 2021. Response of a Small River Plume on Wind Forcing. Frontiers in Marine Science, (8), 809566. https://doi.org/10.3389/fmars.2021.809566
- Kondratev, S.I., 2019. Three Typical Hydrological-Hydrochemical Situations near the Danube River Mouth Based on the Marine Hydrophysical Institute Research Expeditions in 1997-2013. Physical Oceanography, 26(4), pp. 326-340. https://doi.org/10.22449/1573-160X-2019-4-326-340
- 4. Osadchiev, A.A., 2021. River Plumes. Moscow: Scientific World, 286 p. (in Russian).
- 5. Zhurbass, V.M., Zavyalov, P.O., Sviridov, A.S., Lyzhkov, D.A. and Andrulionis, E.E., 2011. [On the Transport of Small River Runoff by Coastal Baroclinic Sea Currents]. *Okeanologiya*, 51(3), pp. 440-449 (in Russian).
- 6. Whitehead, J.A., 1985. The Deflection of a Baroclinic Jet by a Wall in a Rotating Fluid. *Journal of Fluid Mechanics*, 157, pp. 79-93. https://doi.org/10.1017/S0022112085002312
- Garvine, R.W., 1987. Estuary Plumes and Fronts in Shelf Waters: A Layer Model. *Journal of Physical Oceanography*, 17(11), pp. 1877-1896. https://doi.org/10.1175/1520-0485(1987)017<1877:EPAFIS>2.0.CO;2
- 8. Garvine, R.W., 1995. A Dynamical System for Classifying Buoyant Coastal Discharges. Continental Shelf Research, 15(13), pp. 1585-1596. https://doi.org/10.1016/0278-4343(94)00065-U
- 9. Yankovsky, A.E. and Chapman, D.C., 1997. A Simple Theory for the Fate of Buoyant Coastal Discharges. *Journal of Physical Oceanography*, 27(7), pp. 1386-1401. https://doi.org/10.1175/1520-0485(1997)027<1386:ASTFTF>2.0.CO;2
- 10. Horner-Devine, A.R., Hetland, R.D. and MacDonald, D.G., 2015. Mixing and Transport in Coastal River Plumes. *Annual Review of Fluid Mechanics*, 47(1), pp. 569-594. https://doi.org/10.1146/annurev-fluid-010313-141408
- 11. Mikhailov, V.N., Mikhailova, M.V. and Frolova, N.L., 1985. Mixing of River and Sea Waters at the Mouth of a Large River. *Vestnik Moskovskogo Universiteta. Seria 5: Geografia*, (6), pp. 37-42 (in Russian).
- 12. Garvine, R.W., 1974. Physical Features if the Connecticut River Outflow during High Discharge. *Journal of Geophysical Research*, 79(6), pp. 831-846. https://doi.org/10.1029/JC079i006p00831
- 13. Horner-Devine, A.R., 2009. The Bulge Circulation in the Columbia River Plume. *Continental Shelf Research*, 29(1), pp. 234-251. https://doi.org/10.1016/j.csr.2007.12.012
- 14. Kourafalou, V.H. and Stanev E.V., 2001. Modeling the Impact of Atmospheric and Terrestrial Inputs on the Black Sea Coastal Dynamics. *Annales Geophysicae*, 19(2), pp. 245-256. https://doi.org/10.5194/angeo-19-245-2001
- 15. Yankovsky, A.E., Lemeshko, E.M. and Ilyin, Yu.P., 2004. The Influence of Shelfbreak Forcing on the Alongshelf Penetration of the Danube Buoyant Water, Black Sea. *Continental Shelf Research*, 24(10), pp. 1083-1098. https://doi.org/10.1016/j.csr.2004.03.007

- Avicola, G. and Huq, P., 2002. Scaling Analysis for the Interaction between a Buoyant Coastal Current and the Continental Shelf: Experiments and Observations. *Journal of Physical Oceanography*, 32(11), pp. 3233-3248. https://doi.org/10.1175/1520-0485(2002)032<3233:SAFTIB>2.0.CO;2
- Miladinova, S., Stips, A., Macias Moy, D. and Garcia-Gorriz, E., 2020. Pathways and Mixing of the North Western River Waters in the Black Sea. *Estuarine, Coastal and Shelf Science*, 236, 106630. https://doi.org/10.1016/j.ecss.2020.106630
- 18. Ivanov, V.A., Kubryakov, A.I., Mikhailova, E.N. and Shapiro, N.B., 1996. Modeling of River Discharge Freshening Effect during Spring Flood at the Black Sea Northwestern Shelf. *Izvestiya, Atmospheric and Oceanic Physics*, 32(1), pp. 140-148.
- Dinu, I., Bajo, M., Umgiesser, G. and Stănică, A., 2017. Romanian Coastal Dynamics during Cold and Warm Seasons Analyzed by Means of a Numerical Model. *Geo-Eco-Marina*, 23, pp. 71-102. https://doi.org/10.5281/zenodo.1194142
- Tsyganova, M.V. and Lemeshko, E.M., 2021. Interannual Variability of the Wind Field on the Black Sea North Western Shelf and Its Impact on River Plume Formation for Decade 2011– 2020. In: SPIE, 2021. Proceedings of SPIE. 27th International Symposium on Atmospheric and Ocean Optics, Atmospheric Physics. Moscow: SPIE. Vol. 11916, 119163G. https://doi.org/10.1117/12.2603268
- 21. Simonov, A.I. and Altman, E.I., eds., 1991. *Hydrometeorology and Hydrochemistry of the Seas of the USSR. Vol. IV. Black Sea. Issue 1. Hydrometeorological Conditions.* Leningrad: Hydrometeoizdat, 429 p. (in Russian).
- 22. Kosarev, A.N., Arkhipkin, V.S. and Katysheva, M.V., 2001. Hydrological Structure of the Waters in the Northwestern Part of the Black Sea. *Vestnik Moskovskogo Universiteta, Seriya 5: Geografiya*, (5), pp. 50-54 (in Russian).
- 23. Jaoshvili, Sh., 2002. The *Rivers of the Black Sea*. Tbilisi: European Environment Agency, 58 p. (Technical Report No. 71).
- Tsyganova, M.V., Zavialov, P.O. and Lemeshko, E.M., 2018. The Interannual Variability of Suspended Matter Concentration in the North-Western Part of the Black Sea. In: SPIE, 2018. Proceedings of SPIE. 24th International Symposium on Atmospheric and Ocean Optics: Atmospheric Physics. Tomsk: SPIE. Vol. 10833, 1083328. https://doi.org/10.1117/12.2504485
- Kurkin, A., Kurkina, O., Rybin, A. and Talipova, T., 2020. Comparative Analysis of the First Baroclinic Rossby Radius in the Baltic, Black, Okhotsk, and Mediterranean Seas. *Russian Journal* of Earth Sciences, 20(4), ES4008. https://doi.org/10.2205/2020ES000737
- 26. Hickey, B.M., Pietrafesa, L.J., Jay, D.A. and Boicourt, W.C., 1998. The Columbia River Plume Study: Subtidal Variability in the Velocity and Salinity Fields. *Journal of Geophysical Research: Oceans*, 103(C5), pp. 10339-10368. https://doi.org/10.1029/97JC03290
- 27. Murray, S.P., ed., 1998. *An Observational Study of the Mississippi-Atchafalaya Coastal Plume. Final Report.* New Orleans, LA: US Department of the Interior, 544 p. (OCS Study MMS 98-0040).
- 28. Fong, D.A. and Geyer, W.R., 2002. The Alongshore Transport of Freshwater in a Surface-Trapped River Plume. *Journal of Physical Oceanography*, 32(3), pp. 957-972. https://doi.org/10.1175/1520-0485(2002)032<0957:TATOFI>2.0.CO;2
- Karageorgis, A.P., Kourafalou, V.H., Anagnostou, C., Tsiaras, K.P., Raitsos, D.E., Papadopoulos, V. and Papadopoulos, A., 2009. River-Induced Particle Distribution in the Northwestern Black Sea (September 2002 and 2004). *Journal of Geophysical Research: Oceans*, 114(C12), C12003. https://doi.org/10.1029/2009JC005460
- 30. Fomin, V.V. and Polozok, A.A., 2022. Features of River Plume Formation in a Shallow Lagoon (the Case of the Sivash Bay, the Sea of Azov). *Ecological Safety of the Coastal and Shelf Zones of the Sea*, (3), pp. 28-42. https://doi.org/10.22449/2413-5577-2022-3-28-42
- 31. Ivanov, V.A. and Fomin, V.V., 2008. [Mathematical Modeling of Dynamic Processes in Sea-Land Area]. Sevastopol, ECOSI-Gidrofizika, 363 p. (in Russian).

- 32. Tsyganova, M.V., Lemeshko, E.M. and Ryabtsev, Yu.N., 2023. Influence of Upwelling on River Plume Development in the Coastal Zone of the North-Western Black Sea Shelf Based on Numerical Modelling. *Ecological Safety of Coastal and Shelf Zones of Sea*, (1), pp. 20-30. https://doi.org/10.22449/2413-5577-2023-1-20-30
- Fofonova, V., Kärnä, T., Klingbeil, K., Androsov, A., Kuznetsov, I., Sidorenko, D., Danilov, S., Burchard, H. and Wiltshire, K.H., 2021. Plume Spreading Test Case for Coastal Ocean Models. Geoscientific Model Development, 14(11), pp. 6945-6975. https://doi.org/10.5194/gmd-14-6945-2021

Submitted 17.03.2025; approved after review 19.05.2025; accepted for publication 11.07.2025.

About the authors:

Marina V. Tsyganova, Junior Researcher, Marine Hydrophysical Institute of RAS (2 Kapitanskaya Str., Sevastopol, 299011, Russian Federation), ORCID ID: 0000-0003-2398-1756, ResearcherID: S-5426-2018, m.tsyganova@mhi-ras.ru

Evgeniy M. Lemeshko, Leading Researcher, Marine Hydrophysical Institute of RAS (2 Kapitanskaya Str., Sevastopol, 299011, Russian Federation), ORCID ID: 0000-0003-4676-1940, ResearcherID: S-7815-2018, evgeny.lemeshko@mhi-ras.ru

Vladimir V. Fomin, Chief Researcher, Marine Hydrophysical Institute of RAS (2 Kapitanskaya Str., Sevastopol, 299011, Russian Federation), DSc. (Phys.-Math.), ORCID ID: 0000-0002-9070-4460, v.fomin@mhi-ras.ru

Yuriy N. Ryabtsev, Researcher, Marine Hydrophysical Institute of RAS (2 Kapitanskaya Str., Sevastopol, 299011, Russian Federation), ORCID ID: 0000-0002-9682-9969, ruab@mail.ru

Contribution of the co-authors:

Marina V. Tsyganova – review, systematization and analysis of literary sources, conducting numerical experiments, processing, analysis of numerical modeling data, description of results, preparation of text and graphic materials for the article

Evgeniy M. Lemeshko – statement of the problem, processing, analysis and description of the research results, preparation of the text of the article

Vladimir V. Fomin – preparation of a numerical model, selection and justification of methods for solving equations and preparation of an article

Yuriy N. Ryabtsev – conducting numerical runs, analyzing the modeling results and preparing the article

The authors have read and approved the final manuscript. The authors declare that they have no conflict of interest.